Published in final edited form as:
Psychiatry Res. 2014 March 30; 221(3): 220–230. doi:10.1016/j.pscychresns.2014.01.005.

Chronic Cocaine Administration Causes Extensive White Matter Damage in Brain: Diffusion Tensor Imaging and Immunohistochemistry Studies

Ponnada A. Narayana[a,*], **Juan J. Herrera**[a], **Kurt H Bockhorst**[a], **Emilio Esparza-Coss**[a], **Ying Xia**[a], **Joel L. Steinberg**[b], and **F. Gerard Moeller**[b]

[a]Department of Diagnostic and Interventional Imaging, University of Texas Health Science Center at Houston, Houston, TX, USA

[b]Department of Psychiatry, Virginia Commonwealth University School of Medicine, Richmond, VA, USA

Abstract

The effect of chronic cocaine exposure on multiple white matter structures in rodent brain was examined using diffusion tensor imaging (DTI), locomotor behavior, and end point histology. The animals received either cocaine at a dose of 100 mg/kg (N=19), or saline (N=17) for 28 days through an implanted osmotic minipump. The animals underwent serial DTI scans, locomotor assessment, and end point histology for determining the expressions of myelin basic protein (MBP), neurofilament-heavy protein (NF-H), proteolipid protein (PLP), Nogo-A, aquaporin-4 (AQP-4), and growth associated protein – 43 (GAP-43). Differences in the DTI measures were observed in the splenium (scc) and genu (gcc) of the corpus callosum (cc), fimbria (fi), and the internal capsule (ic). Significant increase in the activity in the fine motor movements and decrease in the number of rearing events were observed in the cocaine treated animals. Reduced MBP and Nogo-A, and increased GAP-43 expressions were most consistently observed in these structures. A decrease in the NF-H expression was observed in fi and ic. The reduced expression of Nogo-A and increased GAP-43 may suggest destabilization of axonal connectivity and increased neurite growth with aberrant connections. Increased GAP-43 suggests drug induced plasticity or a possible repair mechanism response. The findings indicated that multiple white matter tracts are affected following chronic cocaine exposure.

Keywords

magnetic resonance imaging; diffusion tensor imaging; cocaine; rodents; immunohistochemistry; neurobehavioral assay

1 INTRODUCTION

Cocaine is a potent stimulant drug of abuse that can result in behavioral and neurochemical changes in preclinical studies (Stankeviciute et al., 2013). In humans, cocaine abuse is also associated with changes in brain structure and function (Moeller et al., 2005; Poon et al., 2007; Ma et al., 2009). Earlier neurochemical studies on the effects of cocaine abuse focused

*Corresponding Author, Ponnada Narayana, PhD, Professor and Director, Department of Diagnostic and Interventional Imaging, University of Texas Medical School at Houston, Houston, TX 77030, Phone: (713) 500-7677, Ponnada.a.narayana@uth.tmc.edu.

FINANCIAL DISCLOSURE
None of the authors has any financial disclosure to make.

on the brain gray matter (GM) structures. For example, it was shown that myelin proteins are significantly decreased in the nucleus accumbens, which is implicated in addiction (Kovalevich et al., 2012).

Recent studies also found that cocaine affects white matter (WM) integrity. Diffusion tensor imaging (DTI) studies showed evidence of structural alterations in cocaine users in the corpus callosum (cc) (Lim et al., 2002; Moeller et al., 2005; Moeller et al., 2007; Ma et al., 2009; Lane et al., 2010). These impairments seen on DTI appear to be associated with high levels of impulsivity, poor cognitive control, and mental flexibility (Moeller et al., 2005). Human studies, based on the DTI derived transverse or radial diffusivity (RD) measurements have also suggested that chronic cocaine use may be associated with compromised myelin integrity (Moeller et al., 2007), consistent with mRNA and histology findings (Bannon et al., 2005).

Our controlled studies investigated if these changes in the DTI measures observed in humans can be replicated in the rodent model of cocaine exposure and determined the pathological underpinnings using immunohistochemistry (Narayana et al., 2009). In that study, based on the effects seen in human cocaine users, we focused only on the cc and demonstrated significant changes in the DTI measures and altered expression in myelin basic protein (MBP) and neurofilament-heavy (NF-H) following chronic cocaine exposure. Previous studies also found similar changes in these proteins in the nucleus accumbens following cocaine administration (Kovalevich et al., 2012). Based on the mRNA studies, a robust and consistent decrease in the expression of myelin-related genes, including MBP, proteolipid protein (PLP), and myelin-associated oligodendrocyte basic protein (MOBP), was observed in the nucleus accumbens following cocaine exposure (Albertson et al., 2004). Some of the published studies also implicated other proteins such as Nogo-A and the growth associated protein-43 (GAP-43). Nogo-A is a protein that has a central role in the inhibition of axonal growth (Chen et al., 2000; GrandPre et al., 2000). Nogo-A is highly expressed in oligodendrocytes and in some neurons in the hippocampus, motor neurons, and dorsal root ganglia (Huber et al., 2002; Schwab, 2002; Meier et al., 2003; Gil et al., 2006; Trifunovski et al., 2006). Nogo-A plays a role in restricting plasticity in the CNS (McGee et al., 2005). Aquaporin-4 (AQP-4) is an integral membrane pore protein that mediates the movement of water (Preston and Agre, 1991) and has been demonstrated to play a role in regulating extracellular cocaine-induced dopamine and glutamate release in brain (Li et al., 2006).

As indicated above, our previous study focused only on DTI and MBP and NF-H expressions in cc in chronic cocaine administration (Narayana et al., 2009). However, based on some of the published studies referenced above, we hypothesized that chronic cocaine administration affects multiple WM structures, besides cc, and a number of proteins. Therefore, the main purpose of these studies was to investigate the effect of chronic cocaine exposure on 1) all the brain WM structures using DTI, 2) the expressions of multiple WM proteins that include MBP, PLP, NF-H, Nogo-A, GAP-43, and AQP-4 using immunohistochemistry, and 3) motor behavior. A further goal of these studies was to relate the DTI changes to altered expressions in various proteins in rodents for gaining an insight into cocaine-induced pathologic changes. In these studies we acquired the DTI data with high spatial resolution (isotropic voxel of 0.27 mm) for reduced partial volume averaging.

2 METHODS

Cocaine Administration

Eight week old male Sprague-Dawley rats in the weight range of 280 g – 300 g (289 g ± 12.18 g) at baseline were included in this study. The animals were divided into two groups: 1) cocaine at a dose of 100 mg/kg (N=17), and 2) saline treated controls (N=19). Cocaine

dissolved in saline or saline alone (control animals) was continuously infused for 28 days through an Alzet osmotic minipump (Model 2ML4, Durect Corp, CA), implanted subcutaneously as described previously (Narayana et al., 2009). The infusion pump was filled with 2 ml of 400 mg/ml of cocaine or 0.9% saline, which served as the control. The pump delivery rate was 2.5 μl/hr. The pump was primed 24 hours prior to implantation by warming in a tube filled with saline at 37°C in a water bath.

2.1 Magnetic Resonance Imaging Acquisition

All MRI scans were performed at baseline (prior to implanting the infusion pump) and weekly thereafter for a period of one month. Thus each animal was scanned at five time points.

For MRI, animals were anesthetized with isoflurane at an induction dose of 4% and were placed on a custom designed Plexiglas bed that was inserted into the magnet bore and were secured with ear and tooth bars. During the scans, the animals were anesthetized with 2% isoflurane in a mixture of air (68%) and oxygen (30%) delivered by a rodent ventilator (Harvard Apparatus, South Natic, MA, USA) through a nose cone. The respiratory rate and rectal temperature were monitored throughout the experiment with a physiologic monitoring unit (Model 1025, SA Instruments, Stonybrook, NY, USA). A pulse oximeter (Model 570–100, SA Instruments, Stonybrook, NY, USA) was used to monitor the heart rate and oxygen saturation levels. An airflow warmer activated by a temperature probe (Model 11007B, SA Instruments) maintained the body temperature at 36°C.

A 7T/30 USR MRI scanner (Bruker BioSpin, Karlsruhe, Germany) with an actively shielded, water-cooled gradient coil system (Model BGA12; 116 mm diameter) capable of producing maximum gradient amplitude of 400 mT m^{-1} with 80 μs rise time was used for image acquisition. The scanner operating system was ParaVision PV5.1. The vendor-supplied birdcage RF coil (Bruker BioSpin, Billerica, MA, USA) with 72 mm internal diameter and 112 mm effective length was used for transmission. An in-house designed and remotely tunable receive only radio frequency (RF) coil (15 mm diameter), was placed over the head of the animal and fixed to the Plexiglas bed. As a quality assurance procedure, prior to each study, using a spin echo sequence, a homogenous water phantom doped with NiCl2 was used to measure the signal-to-noise ratio (SNR) using the macro Auto_snr that is part of the Bruker scanner software. In this method, the mean signal (mean signal) was measured in an ROI of 3 by 3 voxels around the brightest voxels. The noise at the edges and corners of the image was measured. The lowest value (noise) in any of these locations was determined. The SNR was computed as mean signal/noise. In order to account for the effect of acquisition parameters such as slice thickness, bandwidth, number of averages etc., the Auto-snr routine calculates the SNR per unit volume as:

$$SNR/mm^3 = SNR^* \text{ acqfactor}^* \text{ voxel factor}$$

where, voxel factor = 1/(volume in mm^3) and acqfactor = $[256 * 5.12/(\text{acqsize} * \text{acqtime})]^{1/}$, where acqtime is the sampling time in the frequency encoding direction and acqsize is the number of phase encoding steps. The acqfactor is the normalization factor that is calculated for standard acquisition of bandwidth of 50KHz and 256 complex points (20 usec/pt), and 256 × 256 read x phase matrix size. This method yields SNR that is independent of the acquisition parameters and allows comparison across different scanners and with different acquisition parameters. Even though in the current study all the acquisition parameters were kept the same at different time points, we preferred using this method of computing SNR since it is calculated automatically and avoids any possible operator bias. To convert this to the commonly defined SNR in an image, the values reported here should be divided by 7.28.

Localized shimming over the brain was performed using Bruker supplied Field Map with adjustments up to third order shims followed by a fine tuning of the first and second order shims using the PRESS sequence (TE=20ms, TR=2500 ms, TE1=TE2=10 ms, 2048 points with Hermite RF pulses) to consistently achieve water line width of less than 0.1 ppm (full width at half maximum). A spin echo sequence with echo time (TE) = 10 ms and repetition time (TR) = 5000 ms, was used to finely adjust the 90° RF pulse power manually over the central 1 mm axial slice (FOV=80 mm × 80 mm, matrix=128 × 128). The same geometry was used for all other acquisitions with different sequences. For visualizing any anatomical lesions, images were obtained using the dual echo 2D Rapid Acquisition with Relaxation Enhancement (RARE) sequence with the following parameters: number of slices = 28, slice thickness = 0.5 mm, FOV = 35 mm × 35 mm, matrix = 256 × 256, effective TEs = 26 and 78 ms, TR = 5000 ms, Hermite pulse, RARE Factor = 4, spectral bandwidth = 60 KHz, number of dummy scans = 2, number of averages = 2. The total scan time was 10 min 40 s.

Diffusion-weighted images (DWIs) were acquired with a segmented (four shots) 3D EPI sequence, using icosahedral encoding scheme with bipolar gradients along 42 encoding directions (Madi et al., 2005). The other acquisition parameters were: voxel size = 0.27 mm × 0.27 mm × 0.27 mm, FOV = 34.56 mm × 20.00 mm × 9.45 mm, matrix = 128 × 74 × 35, TE = 24.7 ms, TR = 500 ms, Hermite excitation RF pulse (pulse width = 3.6 ms, flip angle = 90°), bandwidth = 250 kHz, number of averages = 1, and partial FT acceleration = 1.5. The EPI scan parameters included double sampling, automatic trajectory adjustment (that also turns on the navigator echoes), and regridding based on the trajectory. The diffusion parameters were: b-value = 800 s/mm^2, diffusion gradient duration = 5 ms, diffusion gradient separation = 10 ms, number of averages without any diffusion gradient (b_0 images) = 9. The total scan time was 1 hr.

2.2 MRI Analysis

The RARE images were mainly used for visualizing anatomical lesions. Other than the routine processing that is a part of the scanner recon software, no additional processing was performed on these images.

An in-house developed pipeline written in IDL software (Exelis Visual Information Solutions, Boulder, CO) was used for automatically processing the DWIs. The pipeline included eddy current correction with the program ‘eddy_correct’, part of the FSL package (Smith et al., 2004), filtering noise and smoothing the data (Hahn et al., 2010), extracting brain using a semi-automatic method, and linear and nonlinear registration with automatic image registration (AIR; Woods et al., 1998a; Woods et al., 1998b) to a template for group analysis. The unregistered images were exported to DtiStudio (Jiang et al., 2006) and the parametric maps of fractional anisotropy (FA), MD, RD, and LD were generated for each animal.

Two levels of analysis were performed: (1) voxel based analysis of FA, and (2) region of interest (ROI) analysis. The voxel based analysis was performed using SPM8 (http://www.fil.ion.ucl.ac.uk/spm/software/) to identify voxels that differ in FA between controls and cocaine animals. Since the only purpose of the SPM8 analysis was to guide in the placement of the ROIs, we did not correct the SPM8 results for multiple comparisons. The final results were based on the ROI analysis. The ROIs were drawn around voxels that showed changes in the tmaps. Even with high isotropic spatial resolution of 0.27 mm, because of the small structure of scc and gcc, we used relatively small ROIs to minimize partial volume averaging effect. The positioning of the ROIs was based on the 3D anatomy. The ROIs were drawn manually on each slice for each animal by the same person who was blind to the treatment. Given the experience of this person (about 15 years of experience in rat neuroanatomy and rodent brain MRI), it is unlikely that the operator bias in the ROI

placement is significant. However, such a bias cannot be completely ruled out. Since the slice orientation varied slightly from animal-to-animal, the ROI size varied slightly (± 2 pixels) to minimize partial volume averaging. For descriptive purposes, the means and standard deviations of the parametric maps of the DTI measures within each ROI were calculated in each animal's native space using the ROI Manager of ImageJ (National Institute of Mental Health, Bethesda, Maryland, USA). Regions that did not show high t-statistic were not included in the ROI analysis. The ROI analysis was performed on each animal (in native space).

2.3 Immunohistochemistry

Immunohistochemistry was performed only over the regions that showed significant differences (either FDR corrected or uncorrected) in any of the DTI measures (see below). On day 28 (end of cocaine delivery with the Alzet pump), following the last MRI scans, animals were transcardially perfused with saline followed by 4% paraformaldehyde in 0.1 M phosphate buffered saline (PBS). The brains were removed and processed as described previously (Narayana et al., 2009). Brains were sectioned at 20 micron thick. Six brain sections, for staining with each primary antibody, spanning the structure of interest from eight randomly selected animals from each group were chosen. These sections were labeled for the following primary antibodies: MBP (1:1000; Covance, CA), NF-H (1:1000; Millipore, Billerica, MA), PLP (1:250; Abcam), Nogo-A (1:1000; Chemicon), AQP-4 (1:1000; Chemicon), and GAP-43 (1:1000, Abcam). Primary antibodies were diluted with blocking solution (0.1 M PBS containing 5% goat serum and 0.3% Triton X-100).

Appropriate secondary antibodies were used at a dilution of 1:500 in 0.1 M PBS. The following Alexafluor dye-conjugated secondary antibodies were used: goat anti-mouse IgG Alexa Fluor® 488 (Invitrogen, Carlsbad, CA) and goat anti-rabbit IgG (H+L) Alex Fluor® 568 (Invitrogen, Carlsbad, CA). The regions included for the immunohistochemistry were scc, gcc, and the body of splenium (bcc), fi, and ic (see below under Results).

2.4 Histology Processing

All images were captured under 20X magnification using a Nikon Eclipse Ni-E microscope (Nikon Instruments; Melville, NY). The exposure times were determined for each antibody in pilot experiments. The threshold levels were set to match those with positive staining and exclude background fluorescence. ImagePro Plus software (Media Cybernetics, Inc.; Silver Spring, MD) was used to measure the percent areas or fluorescent intensity of the antibodies tested and in the region of interest (ROI) as described previously (Herrera et al., 2008; Narayana et al., 2009). The ROIs were placed in scc, bcc, gcc, fi and ic. To ensure consistent analysis between sections, the same ROI size (circular ROI with a 700 μm diameter) was maintained for each section throughout the experiment, and the threshold levels for each primary antibody were determined by random sampling from control sections. Personnel involved in the histologic analyses were blind to the treatment.

2.5 Neurobehavioral Assays

Exploratory behavior that included fine motor movements, ambulation, and rearing activities was assessed using the computerized activity box to assess the general motor behavior (Metz et al., 2000). In this assay animals were placed in the activity chambers for a 30 minute testing period, and the data was collected using the software and hardware provided by the Photobeam Activity System (PAS) with Flexfield (San Diego Instruments, Inc., San Diego, CA). The PAS acquires data on the animal’s movements within the activity chamber by recording the number of photo beams interrupted. The activity can be categorized as fine motor movements, gross movements, and rearing (McMahon and Cunningham, 2001).

Baseline monitoring was performed before the implantation of osmotic pumps, and weekly thereafter, approximately the same time of day for the duration of the study.

2.6 Statistical Analysis

The ROI analysis of the proteins and of the DTI measures other than FA were performed using two-tailed Student's t-test between the control and cocaine exposed groups. Statistical analysis was performed using GraphPad Prism (version 5) software (GraphPad Software, San Diego, CA). The significance level was set at 0.05 for all comparisons. A two-tailed Student's t-test was used to determine differences within each ROI of RD, LD, and the percent of expressions of MBP, NF-H, PLP, GAP-43, AQP-4, and Nogo-A between saline and cocaine administered animals. Group behavioral data and animal weights were analyzed using repeated measure one-way analysis of variance (ANOVA) followed by a Bonferroni multiple comparison correction for the locomotor analysis.

3 RESULTS

3.1 Magnetic Resonance Imaging

The temporal stability of the SNR was excellent, except at a few time points (Fig. 1). No significant artifacts were observed on the images. As can be seen in this figure, low SNR was observed at two time points. We did not investigate the reasons for this low SNR. Data from animals on these two days was not excluded from the final analysis. We did not observe any lesions on the RARE images, indicating that cocaine administration did not result in any gross pathology. Typical T2-weighted RARE images and maps of DTI derived measures are shown in Fig. 2.

3.1.1 DTI: Voxel-based analysis—As an example, the results of the voxel-based analysis are shown in Fig. 3. In this figure, voxels with differences in the FA values between controls and cocaine animals are shown in red (t-maps). These t–maps were generated with (left) and without (right) false discovery rate (FDR) correction for multiple comparisons. With FDR correction, the only regions that showed significant differences (FDR corrected $p < 0.05$) were scc, gcc and ic. However, differences in FA (uncorrected $p < 0.05$) were seen in a few voxels in fi without the FDR correction. It should be pointed out that the t-maps show more extensive injury in the left hemisphere of the brain compared to the right. However, the reasons for this observed asymmetry are unclear.

3.1.2: ROI analysis—The ROI placement was guided by the t-maps that were not corrected for multiple comparisons (Fig. 4 left). The scc and gcc are very small structures in rats. Even though our spatial resolution of 0.27 mm isotropic voxel is one of the highest reported for in vivo rodent studies, we still had to use small number of voxels in a given slice to balance between small number of voxels that could result in statistical noise and large number of voxels that would introduce partial volume averaging. However, the ROI extended to other slices. For ic and fi, ROIs were placed in both hemispheres. The ROI for scc consisted of 28 voxels ($0.55 mm^3$), gcc 71 voxels ($1.4 mm^3$), fi 72 voxels ($1.42 mm^3$), ic 75 voxels ($1.48 mm^3$). As pointed out earlier, the protein analysis and descriptive DTI measures within each ROI were performed in the native space of each animal and thus did not involve registration errors.

Increased RD was observed in scc and fi ($p = 0.0321$). A strong trend towards an increase was observed for RD in gcc ($P = 0.0576$). LD decreased in scc ($p = 0.0339$), gcc ($p = 0.0002$), and ic ($p = 0.0084$). The results of the DTI measures within each ROI are summarized in Fig. 5 and Table1. The error bars in Fig. 5 represent standard deviation.

3.2 Immunohistochemistry

We matched the histology and DTI sections for the ROI analysis as closely as possible by visual inspection, realizing that these two modalities greatly differ in spatial resolution. As an example, Fig. 6 shows the matched histology and DTI sections. As an example, representative immunofluorescence images of fimbria from the control and cocaine treated brains is shown in Fig. 7.

3.2.1 Corpus callosum

3.2.1.1 scc: Immunofluorescent quantification indicated significantly lower MBP ($p = 0.0007$) and Nogo-A ($p = 0.0002$) in the cocaine treated animals compared to the control animals. The cocaine treated animals showed significantly higher GAP-43 expression ($p < 0.0001$) compared to the saline controls. A trend towards a significantly higher expression of NF-H isoform ($p = 0.0506$) and PLP ($p = 0.0801$) was seen in cocaine treated animals. No significant difference in the expression of AQP-4 ($p = 0.2861$) was observed between the two groups. The results of quantitative analysis of the immunofluorescence for scc are shown in Fig. 8. In this figure, the error bars represent standard deviation.

C.2.1.2 gcc: The cocaine treated rats showed significantly lower Nogo-A ($p < 0.0001$), and higher expression of GAP-43 ($p = 0.0151$). A trend towards decrease was observed in the expression of MBP ($p = 0.0637$). Cocaine treated rats showed higher NF-H expression, but this was not statistically significant ($p = 0.2299$). No significant differences were observed in the expressions of PLP ($p = 0.3936$) and AQP-4 ($p = 0.3581$).

C.2.1.3 bcc: We observed no significant differences in MBP ($p = 0.3282$) and Nogo-A ($p = 0.8913$). Similarly, we did not observe significant differences in NF-H ($p = 0.4314$) and AQP-4 ($p = 0.9162$) expression. Cocaine treated rats did however show significantly higher expression of GAP-43 ($p = 0.0445$) and a trend toward statistical significance for PLP ($p = 0.0712$).

C 2.2 fi and ic: We observed a significant decrease in the expression of MBP in both fi ($p < 0.0001$) and ic ($p = 0.001$) in cocaine treated animals compared to controls. Also in the cocaine treated animals there was a significant decrease in the expression of NF-H in fi ($p = 0.0007$) and ic ($p = 0.0015$). An increase in axonal plasticity, as measured by GAP-43, was observed in both fi ($p < 0.0001$) and ic ($p = 0.0011$). There was a significant decrease in the expression of Nogo-A in both fi ($p < 0.0001$) and ic ($p < 0.0001$). No significant difference was observed in the expression of PLP is either the fi ($p = 0.5102$) or ic ($p = 0.7228$). Aquaporin-4 expression was not determined in these regions.

The results of the quantification of immunohistochemical analysis along with the p values for different structures are summarized in Table 2.

3.3 Neurobehavioral assessment

Behavioral assessment indicated a significant increase in the cocaine-treated animals in the activity counts in the fine motor movements compared to baseline measures (Fig 9A). A significant decrease was observed in the number of rearing events in the cocaine treated animals (Fig. 9B). Both these changes were seen at three weeks after the start of cocaine treatment. No significant differences in the ambulatory exploration between the baseline and cocaine administered animals were observed.

4 DISCUSSION

We believe that this is the first comprehensive study that investigated the effects of cocaine using DTI, neurobehavioral assay based on computer activity boxes, and multiple immunohistochemical stains. We observed altered protein expressions in multiple WM structures after chronic administration of cocaine, and differences in DTI metrics, especially RD, in these same brain regions (summarized in Table 1). In addition to confirming our earlier results that scc was affected in cocaine treated animals (Narayana et al., 2009), other WM structures such as fi and ic were also affected by chronic cocaine administration. The implications of these observations are discussed below.

The DTI data indicated differences between cocaine and saline treated rodents in cc and ic. In both of these structures we observed decreased FA, consistent with microstructural changes in the white matter. The reduced MBP expression would suggest compromised myelin, which is consistent with increase RD in the scc and ic (Song et al., 2005; Herrera et al., 2008; Budde et al., 2009; Narayana et al., 2009). In the case of the fi, reduced MBP expression was observed even though a change in RD was not observed. Still, in majority of the structures concomitant changes in both DTI and histological measures were observed.

The LD results were less consistently associated with histopathology across different structures. For example, a decrease in LD was observed in the genu and the splenium of the cc and ic. However, a trend towards increase in NF-H was observed in scc ($p = 0.0506$). This lack of association between LD and NF-H expression is consistent with more recent reports (Budde et al., 2007; DeBoy et al., 2007; Herrera et al., 2008; Budde et al., 2011), which indicate that the original concept of LD being solely related to axonal injury might be overly simplistic.

A robust observation on DTI was increased RD in scc, along with a significant reduction in MBP in the same brain region. The DTI findings are consistent with our previous rodent study and multiple previous human studies in cocaine use (Moeller et al., 2005; Moeller et al., 2007; Narayana et al., 2009). Thus RD could serve as a biomarker of white matter structural damage in cocaine addiction.

The present study demonstrated significantly lower MBP and Nogo-A expressions in scc, gcc, fi and ic, suggesting that myelin compromise extends to multiple WM structures. Among the three substructures of cc, the splenium was most affected, followed by genu. The reasons for this differential effect across the substructures of cc are not completely clear. It was reported that the percentage of myelinated axons showing ultrastructural pathological changes with aging in male Sprague-Dawley rats is much higher in scc compared to gcc and bcc (Sargon et al., 2007b). It was also shown that in this species the number of myelinated axons is higher in the scc compared to gcc and bcc (Sargon et al., 2003). Recent studies also suggest that the axonal caliber is much higher in the bcc compared to gcc and scc (Barazany et al., 2009). Perhaps this suggests that larger axons are less vulnerable to cocaine exposure. In addition, there may be differential expression of proteins involved in lipid peroxidation, oxidative stress, and apoptosis across the cc sub-regions (Kashem et al., 2009).

The internal capsule is also affected by cocaine exposure. Myelin-related transcripts encoding MBP, cyclic nucleotide 3-phosphodiesterase, MAG, and MOG are decreased following cocaine exposure (Kristiansen et al., 2009). The change in ic was also reported on MRI in cocaine subjects (Lim et al., 2008). White matter fibers in ic traverse through basal ganglia allowing connections between the cortex, brainstem, spinal cord, and thalamus. Damage to ic has been demonstrated to correlate with motor impairment in stroke (Pendlebury et al., 1999) and multiple sclerosis (Lee et al., 2000). Our neurobehavorial data

also suggests impairment in rearing activity, which may indicate damage to the corticospinal tract that traverses through posterior limb of the ic.

The fimbria is a major route for afferent and efferent fibers of the hippocampal formation. It plays a critical role as a pathway between the hippocampus and nucleus accumbens, possibly in regulating cocaine seeking behavior (Sabeti et al., 2003; Russo et al., 2010; Kovalevich et al., 2012). Published studies indicate that glutamate excitotoxicity induces apoptosis in oligodendrocytes through an increased caspase-3 cleavage (McDonald et al., 1998; Sanchez-Gomez et al., 2011; Kovalevich et al., 2012). One might speculate that the altered state of myelin observed in fi reflects changes occurring to the glutamatergic pathway.

An interesting observation in our study is the reduced expression of Nogo-A. Reduced Nogo-A promotes neuronal sprouting that could be beneficial in traumatic injury (Liebscher et al., 2005) and early stages of Alzheimer's disease, by compensating for the synaptic loss. However, in the later part of the disease, the sprouting axons may cause aberrant connections that result in further neurodegeneration (Hashimoto and Masliah, 2003). Nogo-A is also shown to stabilize axonal connectivity (Park et al., 2010; Schwab, 2010).

Our findings of reduced Nogo-A are similar to the results of another study that examined WM changes following amphetamine exposure (Yang et al., 2011). That study demonstrated a significant decrease in the oligodendrocyte marker, MBP, Nogo-A, and glutathione S-transferase in the frontal cortex and cc in animals treated with amphetamine, suggesting that different stimulants may exert similar effects on myelin related proteins.

Overall, chronic cocaine exposure produces several changes in various proteins that ultimately lead to white matter injury. One potential mechanism through which cocaine could exert its damaging effects on WM is oxidative stress. Cocaine exposure induces oxidative stress without apoptosis in the rodent frontal cortex and striatum (Dietrich et al., 2005), increases the amount of dopamine in the synaptic cleft, which is metabolized by auto-oxidation or monoamine oxidase, thus increasing reactive oxygen species (ROS) production (Hermida-Ameijeiras et al., 2004). A recent study indicated that Nogo-A has neuroprotective effects against oxidative stress (Mi et al., 2012). Amino-Nogo-A was demonstrated to scavenge reactive oxygen species (ROS) by interacting with oxidized peroxiredoxin 2 in vitro (Mi et al., 2012). Oxidative stress has been demonstrated to precede death of human progenitor cells following cocaine exposure in vitro (Poon et al., 2007). Knockdown of Nogo-A may also cause acute oxidative stress and markedly increase neuronal death (Mi et al., 2012). The possible increased production of ROS combined with the decreased Nogo-A suggests that oxidative stress may be a contributing factor in the pathology observed in our study.

The present study demonstrated a significant increase in the expression of GAP-43. GAP-43 plays a key role in guiding the growth of axons and modulating new connections and enables neurons to sprout new terminals (Aigner et al., 1995). Recent studies demonstrated that decrease in Nogo-A resulted in an increase in axonal plasticity as determined by GAP-43 expression (Dietrich et al., 2005; Masliah et al., 2010). Increased expression of GAP-43 was also observed in the fimbria in prenatal cocaine treated animals (Clarke et al., 1996). In our studies, changes in Nogo-A expression were observed in some structures in the absence of changes in MBP and NFH. This perhaps suggests that GAP-43 is an early indicator of cocaine-induced pathological changes.

It was suggested that late developing WM may be more vulnerable to increased dopamine following amphetamine exposure (Yang et al., 2011). Cocaine administration also produces an increase in extracellular dopamine levels, and changes in WM pathology have been

observed in areas away from cc (Hermida-Ameijeiras et al., 2004; Masliah et al., 2010). Oligodendrocytes express D2 and D3 receptors for dopamine, and stimulation of these receptors resulted in decreased transition of immature oligodendrocytes to mature oligodendrocytes (Bongarzone et al., 1998). In addition to dopamine release, cocaine administration results in alteration of glutamate neurotransmission leading to increased glutamate levels in various brain regions that could alter protein expressions in cc. A follow up study is needed to examine the glutamate levels and the expression of glutamate receptors in cc.

It was demonstrated that repeated chronic administration of cocaine dose resulted in locomotor sensitization (Gulley et al., 2003; Sabeti et al., 2003). The present study has shown that chronic administration of cocaine resulted in an increase in fine motor movements and a decrease in rearing events compared to baseline measures. Increases in fine motor movements were also observed in another study (Wiley et al., 2008). We speculate that the increase in the fine motor movements may be related to the increase in the plasticity in cc but this needs to be examined in a follow-up study. Decreases in rearing events were observed in another chronic cocaine study (van Haaren and Meyer, 1991).

The present study also showed no significant difference between groups in the expression of AQP-4, which has been suggested to be affected in cocaine addiction (Li et al., 2006).

In conclusion, this study extends previous investigation showing an effect of chronic cocaine on brain white matter structure. The findings of reduced expression of Nogo-A and increased levels of GAP-43 could destabilize axonal connectivity and increased neurite growth with aberrant connections. Increased GAP-43 perhaps suggests stimulant induced plasticity or a repair mechanism response. Follow-up studies are needed to gain a better understanding of the cellular and molecular mechanisms underlying the cocaine-induced loss of white matter protein. Understanding the cocaine-induced neuronal plasticity may be critical for identifying novel drug targets for blocking or reversing cocaine induced changes in brain structure and associated behavioral problems.

Acknowledgments

This work is supported National Institute on Drug Abuse (NIDA). Grants #P50 DA009262. NIDA is not responsible for the contents of this manuscript. We thank Mark Mattingly from Bruker for very useful discussions about the SNR measurements.

REFERENCES

Aigner L, Arber S, Kapfhammer JP, Laux T, Schneider C, Botteri F, Brenner HR, Caroni P. Overexpression of the neural growth-associated protein GAP-43 induces nerve sprouting in the adult nervous system of transgenic mice. Cell. 1995; 83:269–278. [PubMed: 7585944]

Albertson DN, Pruetz B, Schmidt CJ, Kuhn DM, Kapatos G, Bannon MJ. Gene expression profile of the nucleus accumbens of human cocaine abusers: evidence for dysregulation of myelin. Journal of Neurochemistry. 2004; 88:1211–1219. [PubMed: 15009677]

Bannon M, Kapatos G, Albertson D. Gene expression profiling in the brains of human cocaine abusers. Addiction Biology. 2005; 10:119–126. [PubMed: 15849025]

Barazany D, Basser PJ, Assaf Y. In vivo measurement of axon diameter distribution in the corpus callosum of rat brain. Brain. 2009; 132:1210–1220. [PubMed: 19403788]

Bongarzone ER, Howard SG, Schonmann V, Campagnoni AT. Identification of the dopamine D3 receptor in oligodendrocyte precursors: potential role in regulating differentiation and myelin formation. Journal of Neuroscience. 1998; 18:5344–5353. [PubMed: 9651217]

Budde MD, Janes L, Gold E, Turtzo LC, Frank JA. The contribution of gliosis to diffusion tensor anisotropy and tractography following traumatic brain injury: validation in the rat using Fourier analysis of stained tissue sections. Brain. 2011; 134:2248–2260. [PubMed: 21764818]

Budde MD, Kim JH, Liang HF, Schmidt RE, Russell JH, Cross AH, Song SK. Toward accurate diagnosis of white matter pathology using diffusion tensor imaging. Magnetic Resonance in Medicine : official journal of the Society of Magnetic Resonance in Medicine/Society of Magnetic Resonance in Medicine. 2007; 57:688–695. [PubMed: 17390365]

Budde MD, Xie M, Cross AH, Song SK. Axial diffusivity is the primary correlate of axonal injury in the experimental autoimmune encephalomyelitis spinal cord: a quantitative pixelwise analysis. Journal of Neuroscience. 2009; 29:2805–2813. [PubMed: 19261876]

Chen MS, Huber AB, van der Haar ME, Frank M, Schnell L, Spillmann AA, Christ F, Schwab ME. Nogo-A is a myelin-associated neurite outgrowth inhibitor and an antigen for monoclonal antibody IN-1. Nature. 2000; 403:434–439. [PubMed: 10667796]

Clarke C, Clarke K, Muneyyirci J, Azmitia E, Whitaker-Azmitia PM. Prenatal cocaine delays astroglial maturation: immunodensitometry shows increased markers of immaturity (vimentin and GAP-43) and decreased proliferation and production of the growth factor S-100. Developmental Brain Research. 1996; 91:268–273. [PubMed: 8852378]

DeBoy CA, Zhang J, Dike S, Shats I, Jones M, Reich DS, Mori S, Nguyen T, Rothstein B, Miller RH, Griffin JT, Kerr DA, Calabresi PA. High resolution diffusion tensor imaging of axonal damage in focal inflammatory and demyelinating lesions in rat spinal cord. Brain. 2007; 130:2199–2210. [PubMed: 17557778]

Dietrich JB, Mangeol A, Revel MO, Burgun C, Aunis D, Zwiller J. Acute or repeated cocaine administration generates reactive oxygen species and induces antioxidant enzyme activity in dopaminergic rat brain structures. Neuropharmacology. 2005; 48:965–974. [PubMed: 15857623]

Gil V, Nicolas O, Mingorance A, Urena JM, Tang BL, Hirata T, Saez-Valero J, Ferrer I, Soriano E, del Rio JA. Nogo-A expression in the human hippocampus in normal aging and in Alzheimer disease. Journal of Neuropathology and Experimental Neurology. 2006; 65:433–444. [PubMed: 16772867]

GrandPre T, Nakamura F, Vartanian T, Strittmatter SM. Identification of the Nogo inhibitor of axon regeneration as a Reticulon protein. Nature. 2000; 403:439–444. [PubMed: 10667797]

Gulley JM, Hoover BR, Larson GA, Zahniser NR. Individual differences in cocaine-induced locomotor activity in rats: behavioral characteristics, cocaine pharmacokinetics, and the dopamine transporter. Neuropsychopharmacology. 2003; 28:2089–2101. [PubMed: 12902997]

Hahn K, Prigarin S, Rodenacker K, Hasan K. Denoising for Diffusion Tensor Imaging with low Signal to Noise Ratios: Method and Monte Carlo Validation. International Journal for Biomathematics and Biostatistics. 2010; 1:63–81.

Hashimoto M, Masliah E. Cycles of aberrant synaptic sprouting and neurodegeneration in Alzheimer's and dementia with Lewy bodies. Neurochemical Research. 2003; 28:1743–1756. [PubMed: 14584828]

Hermida-Ameijeiras A, Mendez-Alvarez E, Sanchez-Iglesias S, Sanmartin-Suarez C, Soto-Otero R. Autoxidation and MAO-mediated metabolism of dopamine as a potential cause of oxidative stress: role of ferrous and ferric ions. Neurochemistry International. 2004; 45:103–116. [PubMed: 15082228]

Herrera JJ, Chacko T, Narayana PA. Histological correlation of diffusion tensor imaging metrics in experimental spinal cord injury. Journal of Neuroscience Research. 2008; 86:443–447. [PubMed: 17868152]

Huber AB, Weinmann O, Brosamle C, Oertle T, Schwab ME. Patterns of Nogo mRNA and protein expression in the developing and adult rat and after CNS lesions. Journal of Neuroscience. 2002; 22:3553–3567. [PubMed: 11978832]

Jiang H, van Zijl PC, Kim J, Pearlson GD, Mori S. DtiStudio: resource program for diffusion tensor computation and fiber bundle tracking. Computer Methods and Programs in Biomedicine. 2006; 81:106–116. [PubMed: 16413083]

Kashem MA, Etages HD, Kopitar-Jerala N, McGregor IS, Matsumoto I. Differential protein expression in the corpus callosum (body) of human alcoholic brain. Journal of Neurochemistry. 2009; 110:486–495. [PubMed: 19457110]

Kovalevich J, Corley G, Yen W, Rawls SM, Langford D. Cocaine-Induced Loss of White Matter Proteins in the Adult Mouse Nucleus Accumbens is Attenuated by Administration of a beta-Lactam Antibiotic during Cocaine Withdrawal. American Journal of Pathology. 2012; 181:1921–1927. [PubMed: 23031254]

Kristiansen LV, Bannon MJ, Meador-Woodruff JH. Expression of transcripts for myelin related genes in postmortem brain from cocaine abusers. Neurochemical Research. 2009; 34:46–54. [PubMed: 18357522]

Lane SD, Steinberg JL, Ma L, Hasan KM, Kramer LA, Zuniga EA, Narayana PA, Moeller FG. Diffusion tensor imaging and decision making in cocaine dependence. PLoS One. 2010; 5:e11591. [PubMed: 20661285]

Lee MA, Blamire AM, Pendlebury S, Ho KH, Mills KR, Styles P, Palace J, Matthews PM. Axonal injury or loss in the internal capsule and motor impairment in multiple sclerosis. Archives of Neurology. 2000; 57:65–70. [PubMed: 10634450]

Li Z, Gao L, Liu Q, Cao C, Sun XL, Ding JH, Hu G. Aquaporin-4 knockout regulated cocaine-induced behavior and neurochemical changes in mice. Neuroscience Letters. 2006; 403:294–298. [PubMed: 16797122]

Liebscher T, Schnell L, Schnell D, Scholl J, Schneider R, Gullo M, Fouad K, Mir A, Rausch M, Kindler D, Hamers FP, Schwab ME. Nogo-A antibody improves regeneration and locomotion of spinal cord-injured rats. Annals of Neurology. 2005; 58:706–719. [PubMed: 16173073]

Lim KO, Choi SJ, Pomara N, Wolkin A, Rotrosen JP. Reduced frontal white matter integrity in cocaine dependence: a controlled diffusion tensor imaging study. Biological Psychiatry. 2002; 51:890–895. [PubMed: 12022962]

Lim KO, Wozniak JR, Mueller BA, Franc DT, Specker SM, Rodriguez CP, Silverman AB, Rotrosen JP. Brain macrostructural and microstructural abnormalities in cocaine dependence. Drug and Alcohol Dependence. 2008; 92:164–172. [PubMed: 17904770]

Ma L, Hasan KM, Steinberg JL, Narayana PA, Lane SD, Zuniga EA, Kramer LA, Moeller FG. Diffusion tensor imaging in cocaine dependence: regional effects of cocaine on corpus callosum and effect of cocaine administration route. Drug and Alcohol Dependence. 2009; 104:262–267. [PubMed: 19595517]

Madi S, Hasan KM, Narayana PA. Diffusion tensor imaging of in vivo and excised rat spinal cord at 7 T with an icosahedral encoding scheme. Magnetic Resonance in Medicine. 2005; 53:118–125. [PubMed: 15690510]

Masliah E, Xie F, Dayan S, Rockenstein E, Mante M, Adame A, Patrick CM, Chan AF, Zheng B. Genetic deletion of Nogo/Rtn4 ameliorates behavioral and neuropathological outcomes in amyloid precursor protein transgenic mice. Neuroscience. 2010; 169:488–494. [PubMed: 20433905]

McDonald JW, Althomsons SP, Hyrc KL, Choi DW, Goldberg MP. Oligodendrocytes from forebrain are highly vulnerable to AMPA/kainate receptor-mediated excitotoxicity. Nature Medicine. 1998; 4:291–297.

McGee AW, Yang Y, Fischer QS, Daw NW, Strittmatter SM. Experience-driven plasticity of visual cortex limited by myelin and Nogo receptor. Science. 2005; 309:2222–2226. [PubMed: 16195464]

McMahon LR, Cunningham KA. Antagonism of 5-hydroxytryptamine(2a) receptors attenuates the behavioral effects of cocaine in rats. Journal of Pharmacology and Experimental Therapeutics. 2001; 297:357–363. [PubMed: 11259563]

Meier S, Brauer AU, Heimrich B, Schwab ME, Nitsch R, Savaskan NE. Molecular analysis of Nogo expression in the hippocampus during development and following lesion and seizure. FASEB J. 2003; 17:1153–1155. [PubMed: 12692091]

Metz GA, Merkler D, Dietz V, Schwab ME, Fouad K. Efficient testing of motor function in spinal cord injured rats. Brain Research. 2000; 883:165–177. [PubMed: 11074045]

Mi YJ, Hou B, Liao QM, Ma Y, Luo Q, Dai YK, Ju G, Jin WL. Amino-Nogo-A antagonizes reactive oxygen species generation and protects immature primary cortical neurons from oxidative toxicity. Cell Death Differ. 2012; 19:1175–1186. [PubMed: 22261619]

Moeller FG, Hasan KM, Steinberg JL, Kramer LA, Dougherty DM, Santos RM, Valdes I, Swann AC, Barratt ES, Narayana PA. Reduced anterior corpus callosum white matter integrity is related to

increased impulsivity and reduced discriminability in cocaine-dependent subjects: diffusion tensor imaging. Neuropsychopharmacology. 2005; 30:610–617. [PubMed: 15637640]

Moeller FG, Hasan KM, Steinberg JL, Kramer LA, Valdes I, Lai LY, Swann AC, Narayana PA. Diffusion tensor imaging eigenvalues: Preliminary evidence for altered myelin in cocaine dependence. Psychiatry Research. 2007; 154:253–258. [PubMed: 17321725]

Narayana PA, Ahobila-Vajjula P, Ramu J, Herrera J, Steinberg JL, Moeller FG. Diffusion tensor imaging of cocaine-treated rodents. Psychiatry Research: Neuroimaging. 2009; 171:242–251.

Park KJ, Grosso CA, Aubert I, Kaplan DR, Miller FD. p75NTR-dependent, myelin-mediated axonal degeneration regulates neural connectivity in the adult brain. Nature Neuroscience. 2010; 13:559–566.

Pendlebury ST, Blamire AM, Lee MA, Styles P, Matthews PM. Axonal injury in the internal capsule correlates with motor impairment after stroke. Stroke. 1999; 30:956–962. [PubMed: 10229727]

Poon HF, Abdullah L, Mullan MA, Mullan MJ, Crawford FC. Cocaine-induced oxidative stress precedes cell death in human neuronal progenitor cells. Neurochemistry International. 2007; 50:69–73. [PubMed: 16956698]

Preston GM, Agre P. Isolation of the cDNA for erythrocyte integral membrane protein of 28 kilodaltons: member of an ancient channel family. Proceedings of the National Academy of Sciences U S A. 1991; 88:11110–11114.

Russo SJ, Dietz DM, Dumitriu D, Morrison JH, Malenka RC, Nestler EJ. The addicted synapse: mechanisms of synaptic and structural plasticity in nucleus accumbens. Trends in Neurosciences. 2010; 33:267–276. [PubMed: 20207024]

Sabeti J, Gerhardt GA, Zahniser NR. Individual differences in cocaine-induced locomotor sensitization in low and high cocaine locomotor-responding rats are associated with differential inhibition of dopamine clearance in nucleus accumbens. Journal of Pharmacology and Experimental Therapeutics. 2003; 305:180–190. [PubMed: 12649367]

Sanchez-Gomez MV, Alberdi E, Perez-Navarro E, Alberch J, Matute C. Bax and calpain mediate excitotoxic oligodendrocyte death induced by activation of both AMPA and kainate receptors. Journal of Neuroscience. 2011; 31:2996–3006. [PubMed: 21414921]

Sargon MF, Celik HH, Aksit MD, Karaagaoglu E. Quantitative analysis of myelinated axons of corpus callosum in the human brain. International Journal of Neuroscience. 2007a; 117:749–755. [PubMed: 17454242]

Sargon MF, Denk CC, Celik HH, Surucu HS, Aldur MM. Electron microscopic examination of the myelinated axons of corpus callosum in perfused young and old rats. International Journal of Neuroscience. 2007b; 117:999–1010. [PubMed: 17613110]

Sargon MF, Mas N, Senan S, Ozdemir B, Celik HH, Cumhur M. Quantitative analysis of myelinated axons of commissural fibers in the rat brain. Anatomia Histologia Embryologia. 2003; 32:141–144.

Schwab ME. Increasing plasticity and functional recovery of the lesioned spinal cord. Progress in Brain Research. 2002; 137:351–359. [PubMed: 12440377]

Schwab ME. Functions of Nogo proteins and their receptors in the nervous system. Nature Reviews of Neuroscience. 2010; 11:799–811.

Smith SM, Jenkinson M, Woolrich MW, Beckmann CF, Behrens TE, Johansen-Berg H, Bannister PR, De Luca M, Drobnjak I, Flitney DE, Niazy RK, Saunders J, Vickers J, Zhang Y, De Stefano N, Brady JM, Matthews PM. Advances in functional and structural MR image analysis and implementation as FSL. Neuroimage. 2004; 23(Suppl 1):S208–S219. [PubMed: 15501092]

Song SK, Sun SW, Ramsbottom MJ, Chang C, Russell J, Cross AH. Dysmyelination revealed through MRI as increased radial (but unchanged axial) diffusion of water. Neuroimage. 2002; 17:1429–1436. [PubMed: 12414282]

Song SK, Yoshino J, Le TQ, Lin SJ, Sun SW, Cross AH, Armstrong RC. Demyelination increases radial diffusivity in corpus callosum of mouse brain. Neuroimage. 2005; 26:132–140. [PubMed: 15862213]

Stankeviciute NM, Scofield MD, Kalivas PW, Gipson CD. Rapid, transient potentiation of dendritic spines in context-induced relapse to cocaine seeking. Addiction Biology. 2013

Trifunovski A, Josephson A, Bickford PC, Olson L, Brene S. Selective decline of Nogo mRNA in the aging brain. Neuroreport. 2006; 17:913–916. [PubMed: 16738487]

van Haaren F, Meyer ME. Sex differences in locomotor activity after acute and chronic cocaine administration. Pharmacology Biochemistry ansd Behavior. 1991; 39:923–927.

Wiley JL, Evans RL, Grainger DB, Nicholson KL. Age-dependent differences in sensitivity and sensitization to cannabinoids and 'club drugs' in male adolescent and adult rats. Addiction Biology. 2008; 13:277–286. [PubMed: 17850418]

Woods RP, Grafton ST, Holmes CJ, Cherry SR, Mazziotta JC. Automated image registration: I. General methods and intrasubject, intramodality validation. Journal of Computer Assisted Tomography. 1998a; 22:139–152. [PubMed: 9448779]

Woods RP, Grafton ST, Watson JD, Sicotte NL, Mazziotta JC. Automated image registration: II. Intersubject validation of linear and nonlinear models. Journal of Computer Assisted Tomography. 1998b; 22:153–165. [PubMed: 9448780]

Yang HJ, Wang L, Cheng Q, Xu H. Abnormal behaviors and microstructural changes in white matter of juvenile mice repeatedly exposed to amphetamine. Schizophrenia Research and Treatment. 2011; 2011:542896. [PubMed: 22937267]

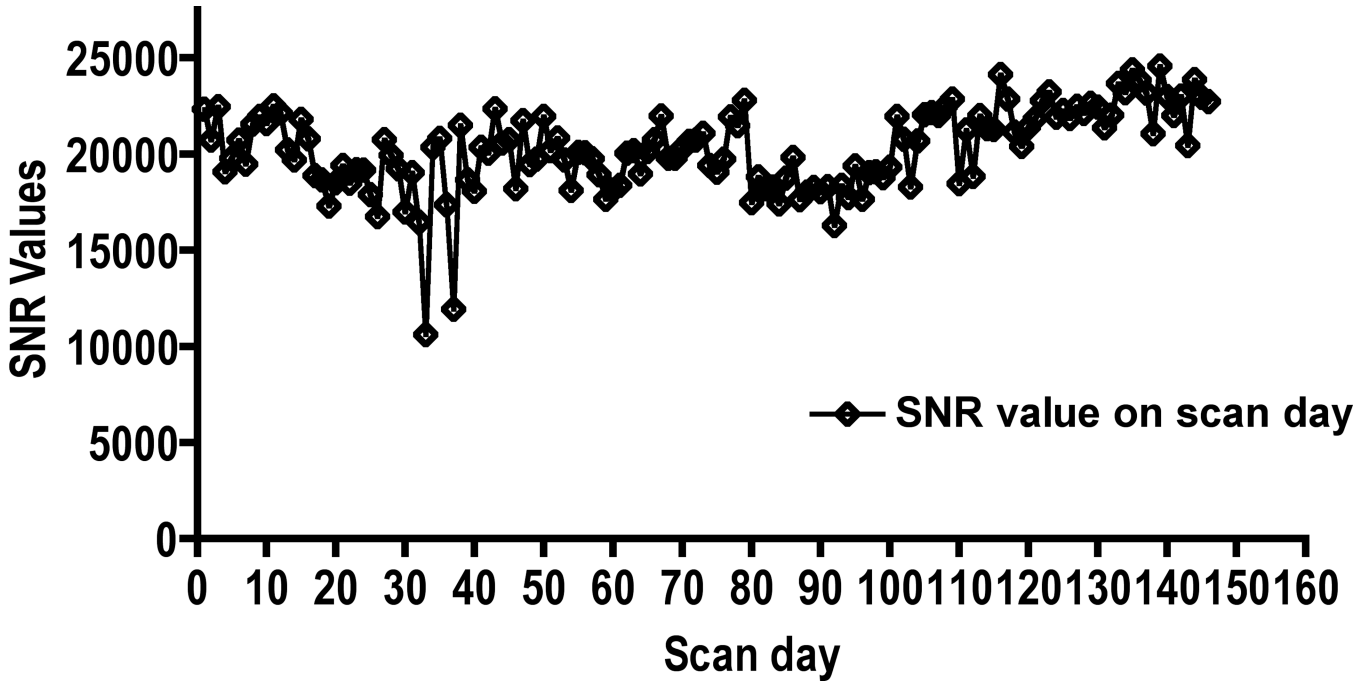

Figure 1.
SNR as a function of time. Overall, the excellent temporal stability in the SNR can be appreciated.

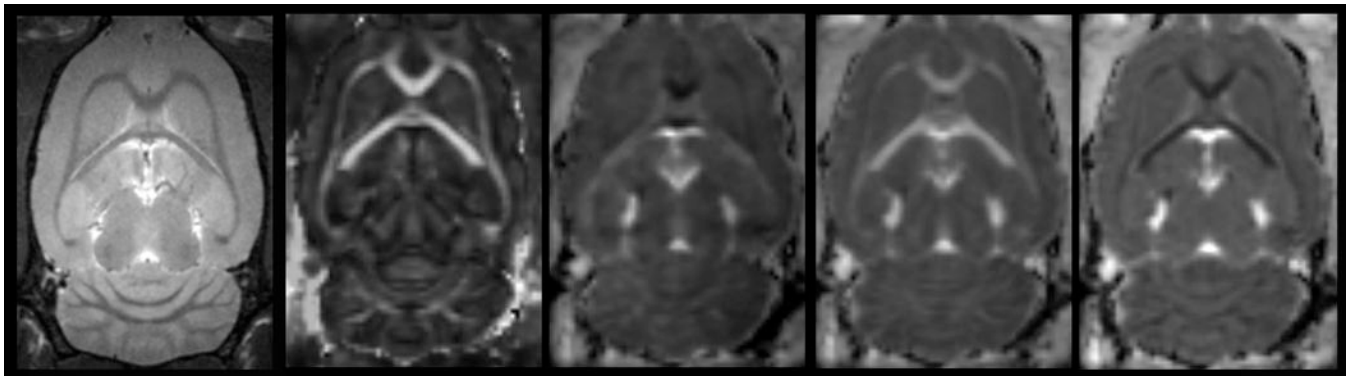

Figure 2.
Multi-modal MRI of three different brain regions (rows) from cocaine exposed animals at the 4 week time point. Representative images of: RARE, fractional anisotropy (FA), mean diffusivity (MD), longitudinal diffusivity (LD), and radial diffusivity (RD).

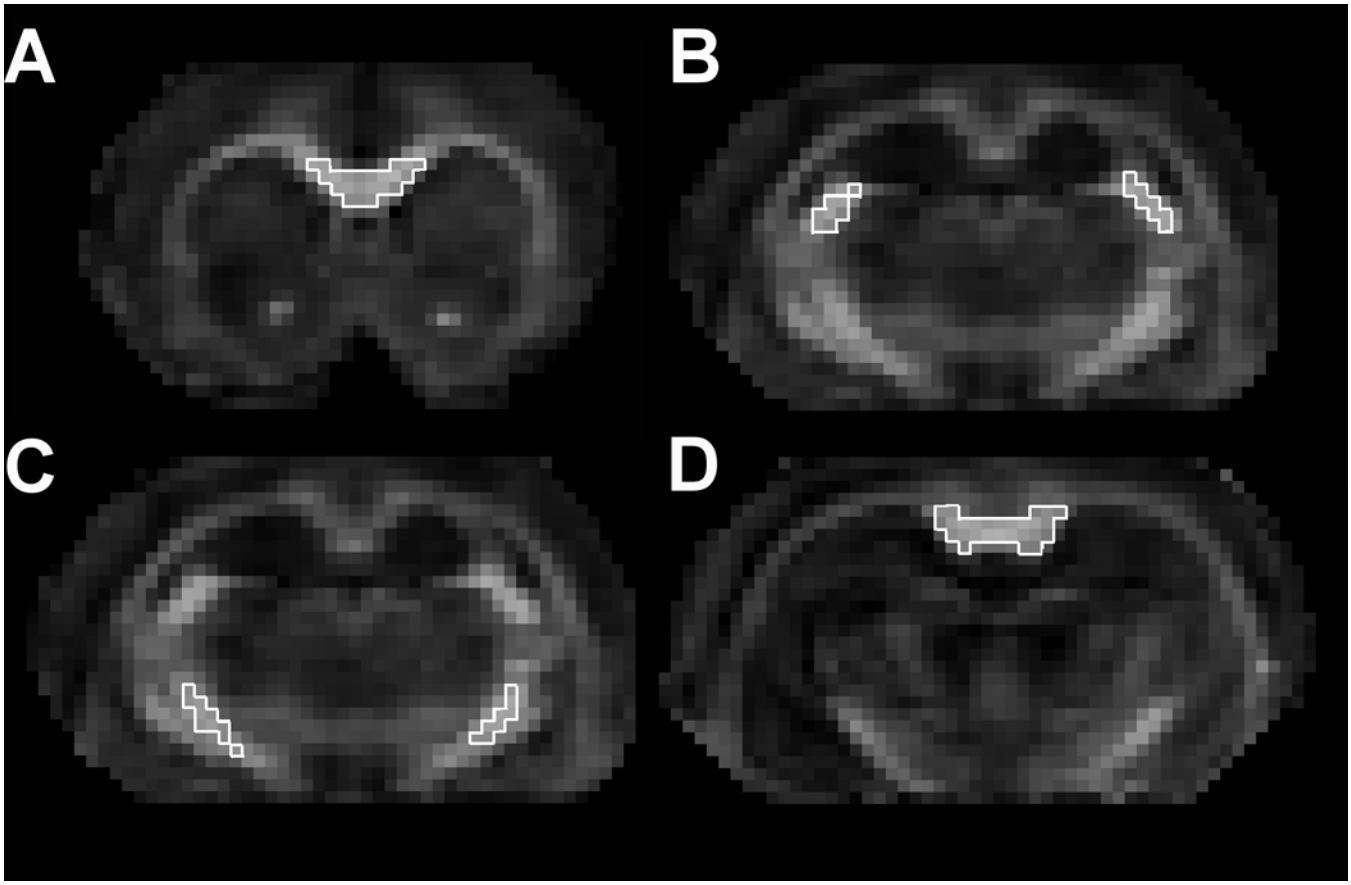

Figure 3.
Representative images showing the placement of the ROI's for comparison between cocaine treated and saline control animals. The ROIs were placed in the (A) genu, (B) fimbria, (C) internal capsule, and (D) splenium.

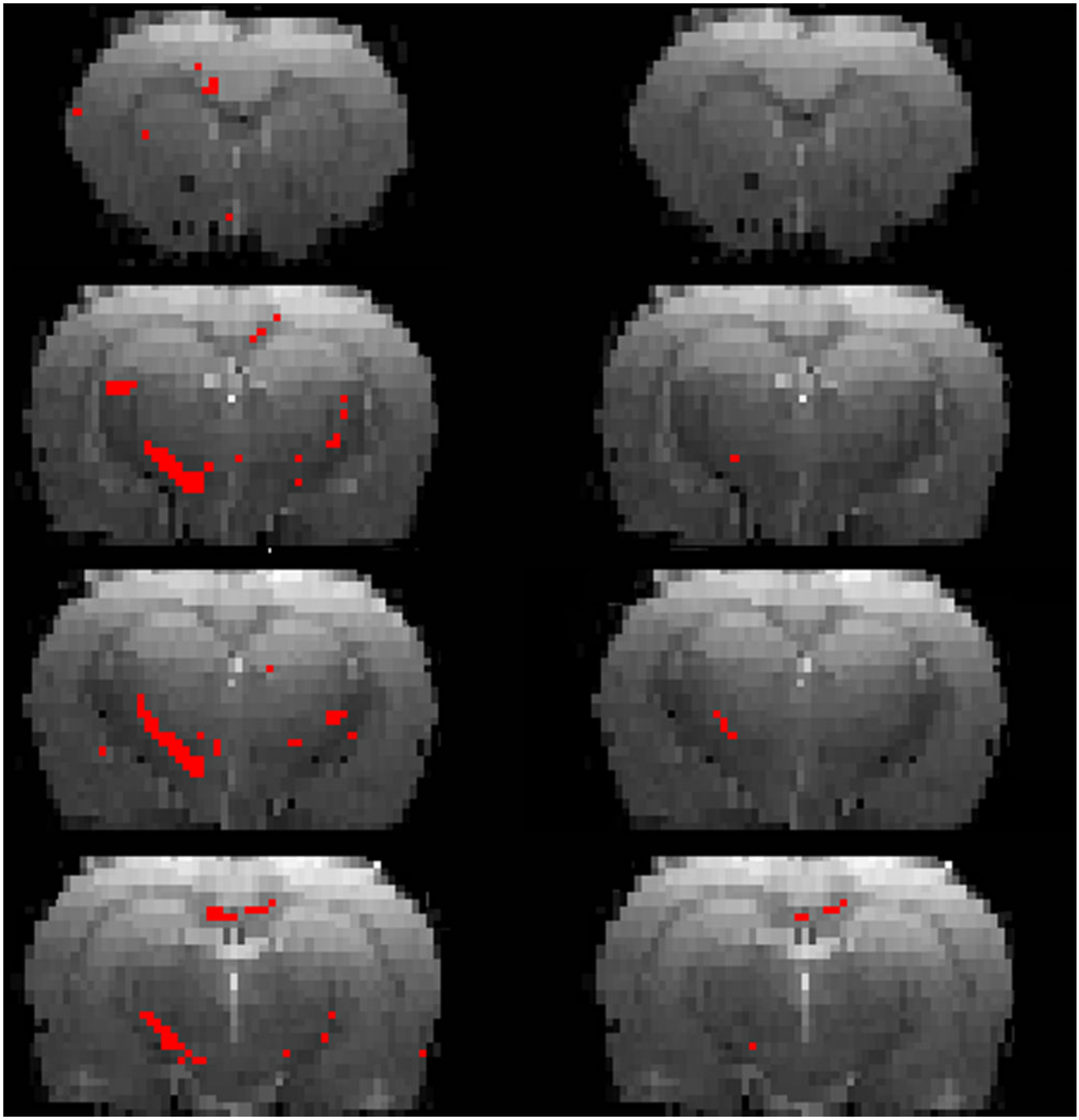

Figure 4.
The t-maps (shown in red) with significantly different FA values between controls and cocaine treated animals superimposed on the RARE images, without (left) and with (right) FDR correction for multiple comparison.

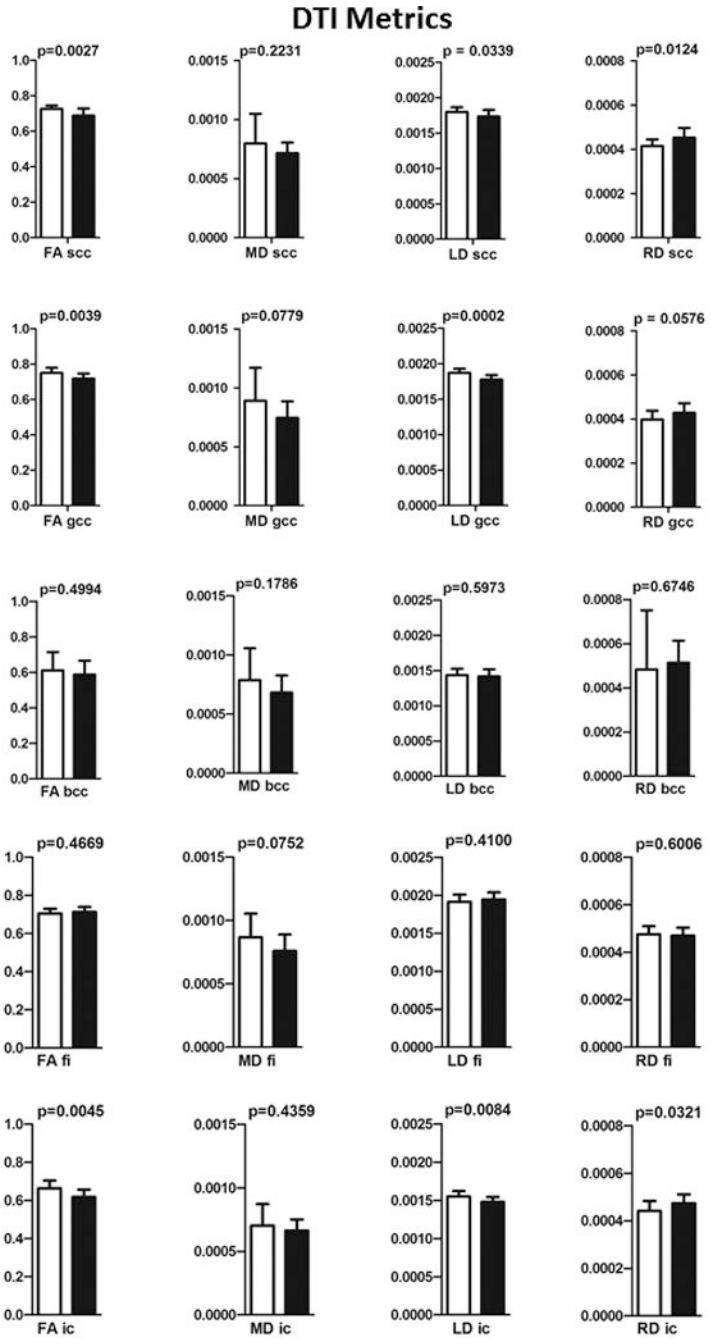

Figure 5.
Results of the ROI analysis of the DTI measures for scc, gcc, bcc, ic, and fi. The p values are also shown in this figure. The error bars represent standard deviation.

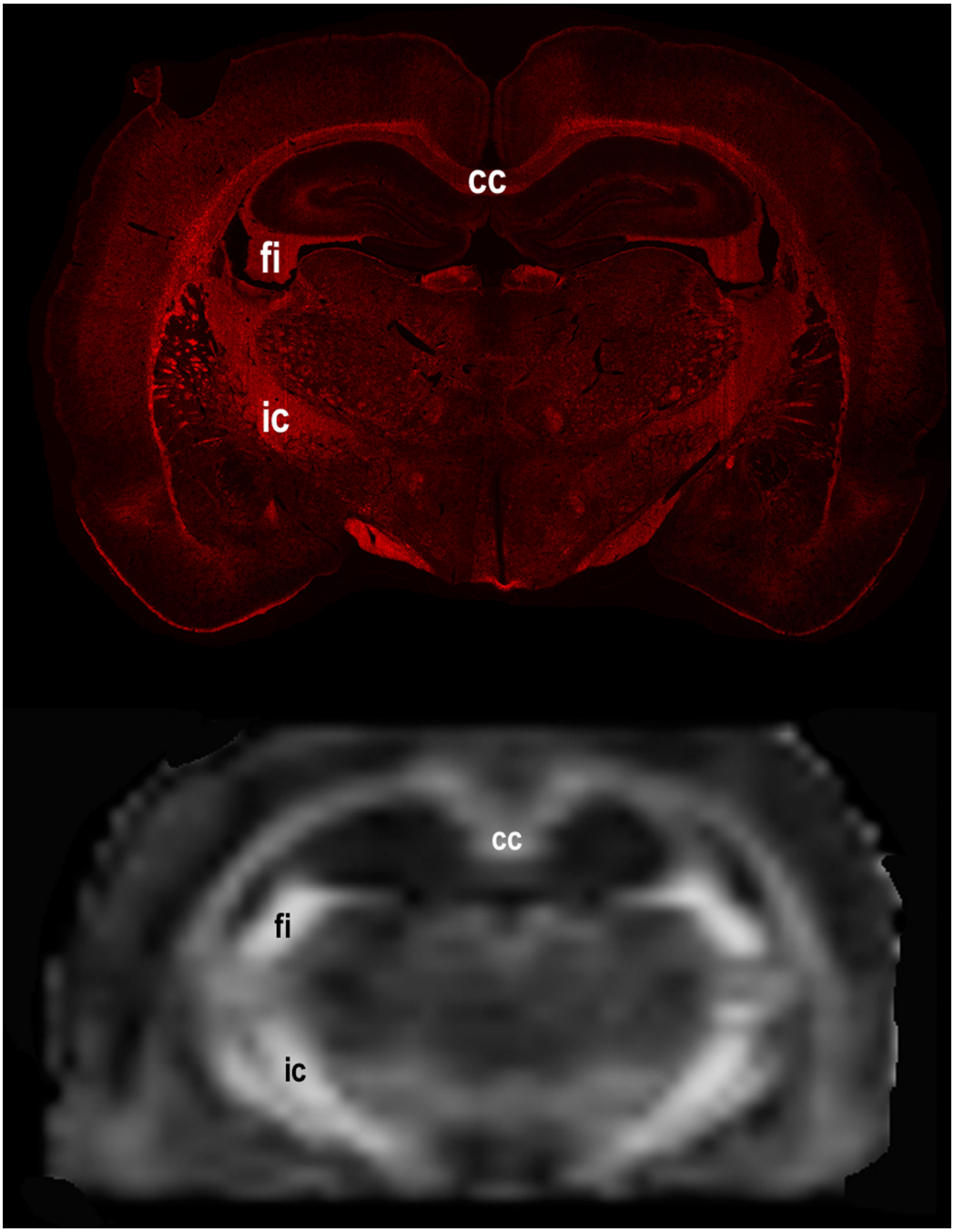

Figure 6.
Representative matched histology and DTI sections in cocaine treated animals. The matching can be seen even with dissimilar spatial resolution.

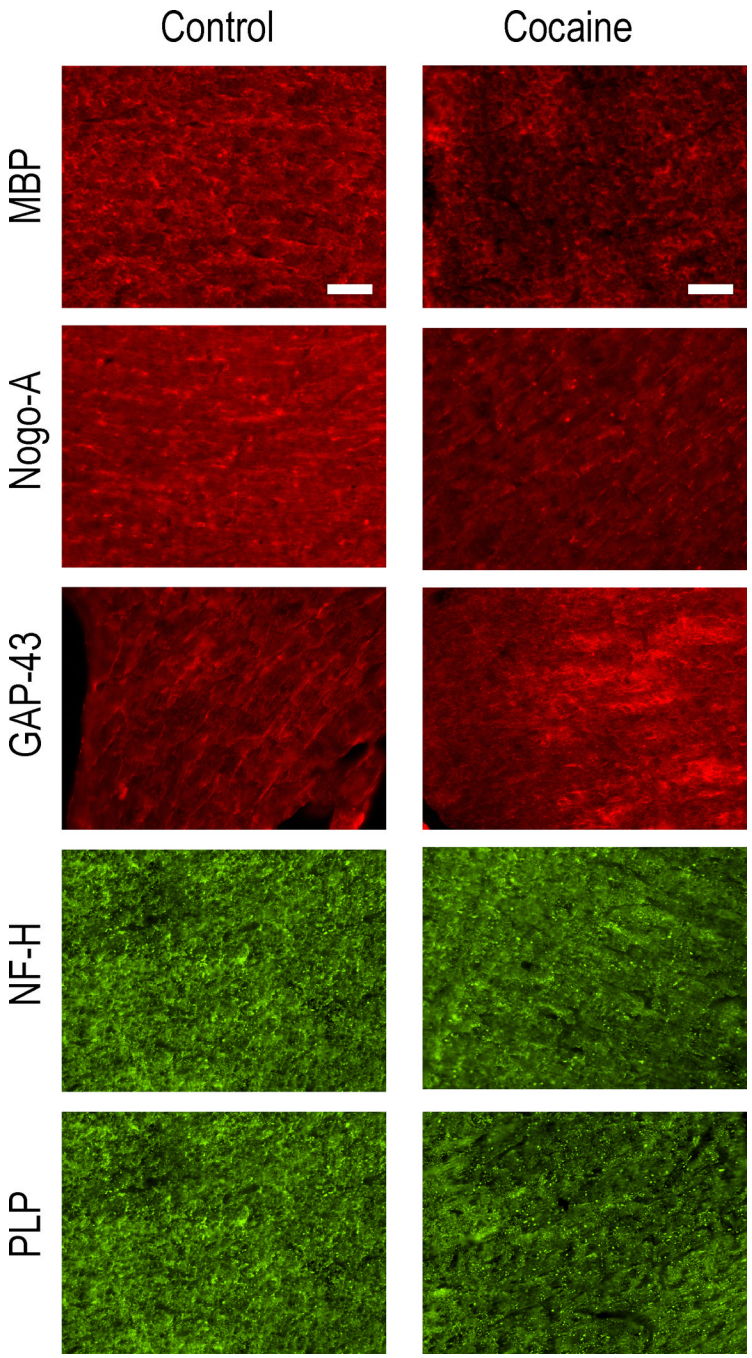

Figure 7.
Representative images of brain sections of the fimbria from control and cocaine exposed brains. The images were obtained to demonstrate the labeling patterns of [panels A and B] myelin basic protein (MBP), [C and D] Nogo-A, [E and F] GAP-43, [G and H] neurofilament – heavy isoform (NF-H), [J and K] proteolipid protein (PLP), and [L and M] aquaporin-4 (AQP-4). scc = splenium. Scale bars = 100 μm.

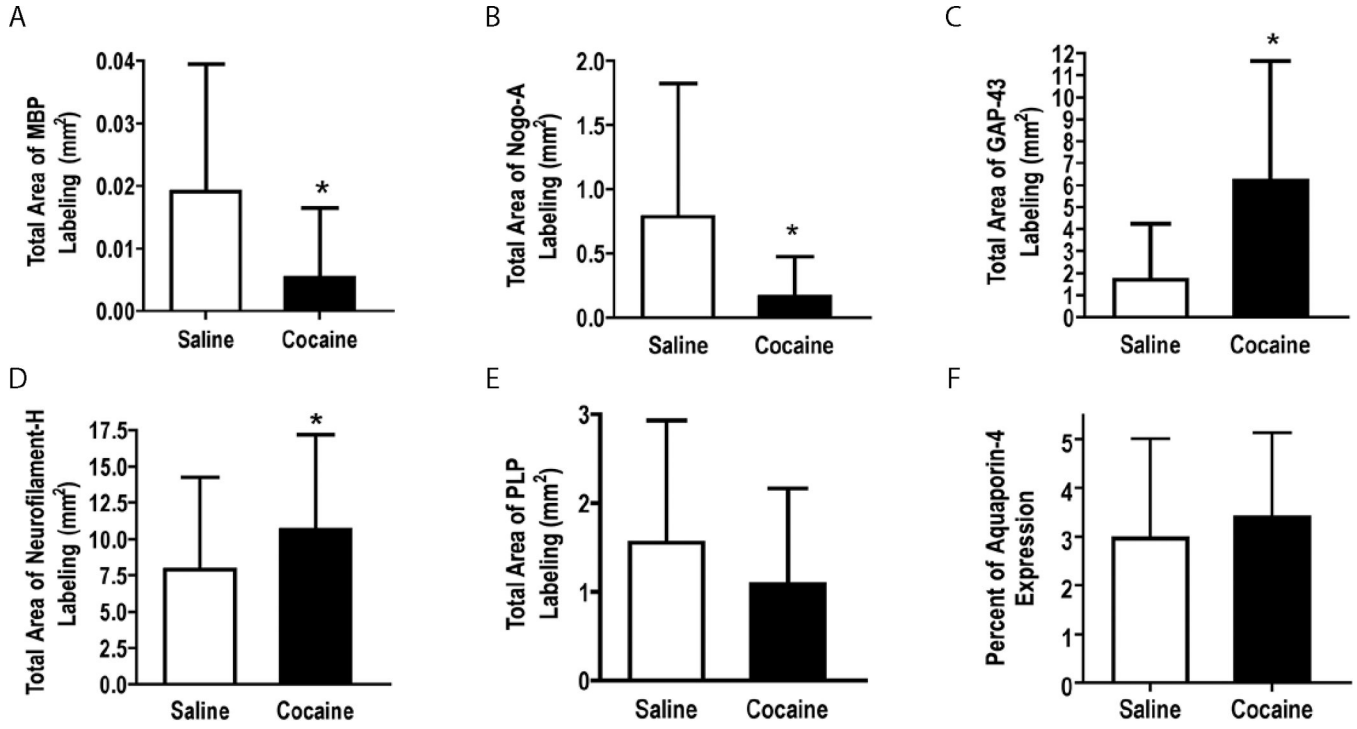

Figure 8.

Quantitative analysis of the expressions of (A) MBP, (B) Nogo-A, (C) GAP-43, (D) NF-H, (E) PLP, and (F) AQP-4 in the splenium of the corpus callosum. A significant decrease was observed in the markers for oligodendrocytes (A & B). A significant increase was observed in GAP-43, a marker of neuronal plasticity. A trend towards statistically significant increase in NF-H was also determined. No significant difference was observed in PLP, and AQP-4 (F). Error bars represent standard deviation.

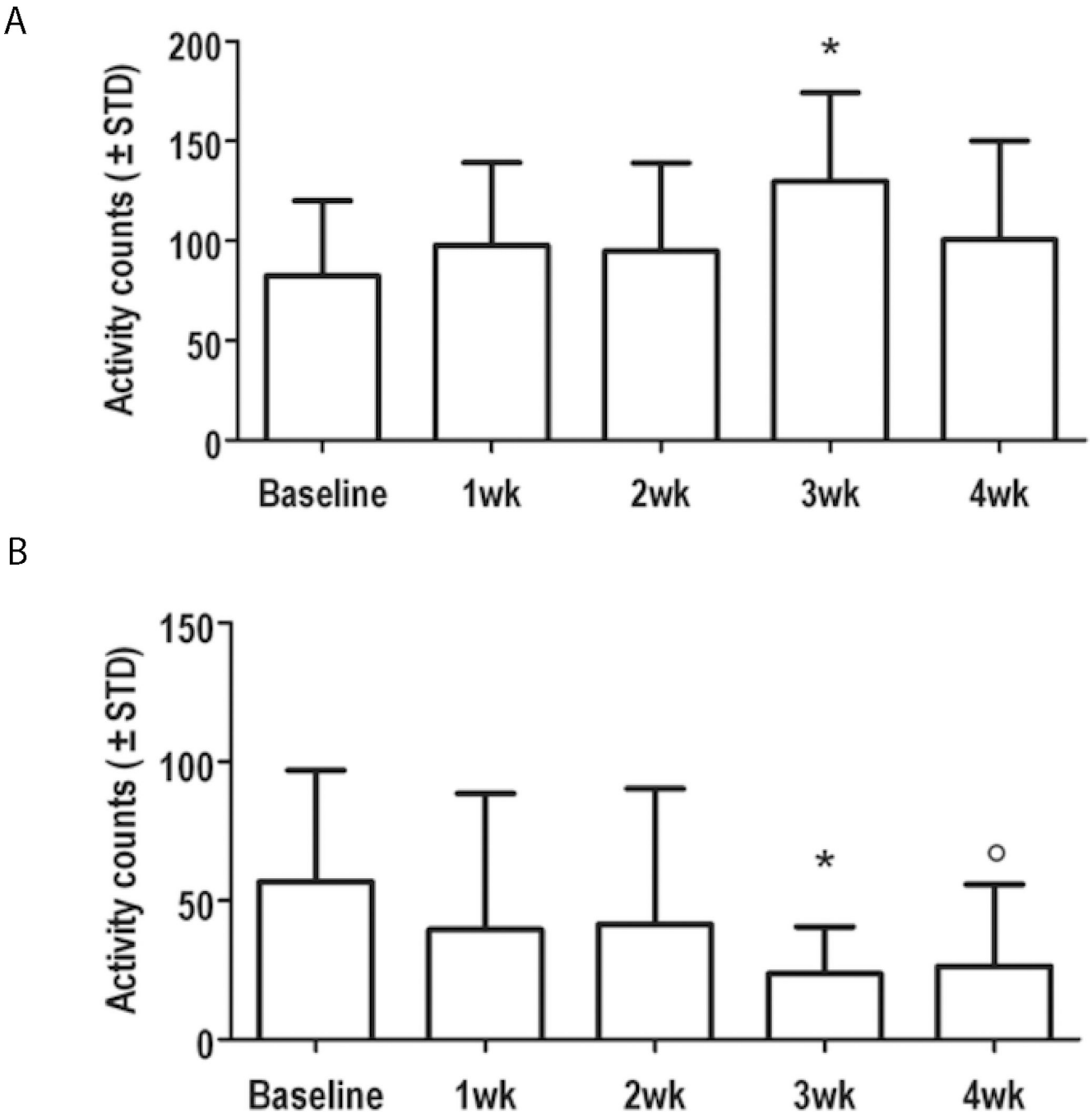

Figure 9.

Motor responses in animals treated with cocaine were compared to baseline measures using computerized activity box monitoring. (A) A significant increase in fine motor movements was observed 3 weeks after chronic cocaine administration compared to baseline measures ($p = 0.0017$). (B) A significant reduction in the number of rearing events was also observed at 3 and 4 weeks of chronic cocaine administration compared to baseline measures ($p = 0.0049$ & 0.0027, respectively).

Table 1

Effect of cocaine treatment on the DTI measures compared to saline. The numerical values represent mean ± sd and the corresponding p values are shown in parenthesis.

DTI Measures	Treatment	White matter structures				
		scc	bcc	gcc	fi	ic
FA (dimensionless)	saline	0.727 ± 0.018	0.612 ± 0.103	0.752 ± 0.028	0.716 ± 0.045	0.661 ± 0.042
	cocaine	0.689 ± 0.040	0.589 ± 0.077	0.719 ± 0.028	0.731 ± 0.039	0.627 ± 0.036
		(0.0027)#	(0.4994)	(0.0039)#	(0.2889)	(0.0119)#
MD ($mm^2s^{-1}*10^{-6}$)	saline	798 ± 250	789 ± 268	890 ± 279	910 ± 204	671 ± 96
	cocaine	715 ± 90	682 ± 146	746 ± 140	817 ± 182	697 ± 149
		(0.2231)	(0.1786)	(0.0779)	(0.1580)	(0.5422)
LD ($mm^2s^{-1}*10^{-6}$)	saline	1797 ± 65	1435 ± 92	1870 ± 57	1921 ± 111	1537 ± 83
	cocaine	1732 ± 91	1416 ± 99	1775 ± 64	1959 ± 90	1482 ± 60
		(0.0339)#	(0.5973)	(0.0002)#	(0.2651)	(0.0280)#
RD ($mm^2s^{-1}*10^{-6}$)	saline	415 ± 30	483 ± 268	397 ± 40	460 ± 57	441 ± 46
	cocaine	449 ± 42	513 ± 99	421 ± 39	446 ± 54	466 ± 37
		(0.0124)*	(0.6746)	(0.0576)	(0.4301)	(0.0806)

and * denote significant decrease and increase (at $p \leq 0.05$) respectively.

Table 2

Effect of cocaine treatment on protein measures compared to saline. The numerical values represent mean ± sd and the corresponding p values are shown in parenthesis.

Protein	Treatment	White matter structures				
		scc	bcc	gcc	ic	fi
MBP	Saline	0.0192 ± 0.02	29.96 ± 21.99	2.044 ± 1.80	7.916 ± 7.77	16.78 ± 13.47
	Cocaine	0.0053 ± 0.01	34.13 ± 19.53	1.431 ± 1.34	5.924 ± 6.29	6.313 ± 5.39
		(0.0007)#	*(0.3282)*	*(0.0637)*	*(0.001)*#	*(<0.0001)*#
Nogo-A	Saline	0.7852 ± 1.04	5.924 ± 11.86	0.7692 ± 0.60	0.9482 ± 1.19	21.20 ± 16.50
	Cocaine	0.1641 ± 0.31	6.260 ± 12.15	0.2494 ± 0.47	0.4592 ± 0.59	9.185 ± 12.20
		(0.0002)#	*(0.8913)*	*(<0.0001)*#	*(<0.0001)*#	*(<0.0001)*#
GAP-43	Saline	1.722 ± 2.54	20.25 ± 28.20	2.233 ± 2.026	1.286 ± 1.91	14.63 ± 8.82
	Cocaine	6.202 ± 5.45	32.94 ± 32.65	3.854 ± 3.90	1.882 ± 2.23	25.54 ± 12.61
		*(<0.0001)**	*(0.0445)**	*(0.0151)**	*(<0.0001)**	*(0.0011)**
NF-H	Saline	7.91 ± 6.35	32.29 ± 24.14	1.100 ± 0.97	4.217 ± 5.81	7.058 ± 6.72
	Cocaine	10.64 ± 6.57	35.96 ± 21.27	1.357 ± 1.05	2.739 ± 4.74	4.282 ± 3.95
		(0.0506)	*(0.4314)*	*(0.2299)*	*(0.0007)*#	*(0.0015)*#
PLP	Saline	1.554 ± 1.38	17.80 ± 18.08	1.239 ± 1.06	3.487 ± 5.06	15.56 ± 14.43
	Cocaine	1.091 ± 1.08	24.29 ± 16.74	1.067 ± 0.85	3.346 ± 3.70	14.23 ± 11.22
		(0.0801)	*(0.0712)*	*(0.3963)*	*(0.7228)*	*(0.5102)*
AQP-4	Saline	2.967 ± 2.04	5.942 ± 4.61	0.984 ± 0.70	ND	ND
	Cocaine	3.394 ± 1.74	6.053 ± 5.71	0.8571 ± 0.63		
		(0.2861)	*(0.9162)*	*(0.3581)*		

and * denote significant decrease and increase (at p≤0.05) respectively.

ND = not determined.